

Chapter 2

***N*-Body Dynamics of Intermediate Mass Ratio Inspirals**

This chapter is adapted from a paper in preparation by *Carl-Johan Haster*, Fabio Antonini, Ilya Mandel and Vicky Kalogera [34]. This paper grew out of a collaboration between the four authors during my pre-doctoral fellowship at the Center for Interdisciplinary Exploration in Astrophysics at Northwestern University. My contribution to this work was (i) initialised, ran and post-processed the *N*-body of the 12 cluster models, (ii) lead the analysis of the results of the IMBH–BH dynamics (iii) wrote the paper.

2.1 Introduction

Intermediate mass black holes (IMBHs) are conjectured to occupy the mass range between stellar-mass black holes (BHs), with masses $\lesssim 100 M_{\odot}$, and supermassive black holes with masses $\gtrsim 10^6 M_{\odot}$ (see [61], for are view). While the existence of some IMBH candidates in dwarf spheroidal galaxies has been conjectured by extending the M – σ relation [28] (but see [50]), dynamical measurements of IMBHs in the few-hundred solar-mass range are extremely challenging (e.g., [67]). The best evidence for such lower mass IMBHs (with mass $\sim 100 M_{\odot}$) could come from ultraluminous X-ray sources (but see [15]); for example, [66] have claimed a mass of $\sim 400 M_{\odot}$ for M82 X-1 from quasi-periodic oscillations, while a mass around $10^4 M_{\odot}$ has been suggested for the brightest ultraluminous X-ray source HLX-1 (e.g., [22, 24, 26]), but these dynamical measurements alone can not provide conclusive proof for the existence of IMBHs.

If these lower-mass IMBHs reside in globular clusters, they will play an important role in cluster dynamics (e.g., [41, 44, 51, 81, 84]). Of particular interest to our study is the likely tendency of IMBHs to dynamically form compact binaries with other compact remnants (e.g., [9, 11, 18, 53–55, 60, 62, 78]). Generally, these analyses find that the IMBH readily captures a binary companion. The binary is subsequently hardened through a sequence of 3-body and 4-body interactions, occasionally with substitutions which make a black hole (BH) of a few tens of solar masses the most

likely IMBH companion, and possible Lidov-Kozai (LK) resonances [42, 45] if hierarchical triples are formed. Eventually, the IMBH-BH binary merges through the radiation of gravitational waves, emitting a signal that is potentially detectable by the Advanced LIGO ground-based GW detectors [3, 33, 35, 76].

Previous simulations of globular clusters with IMBH coalescences have generally simplified the interactions in order to avoid excessive computational cost. For example, Gültekin et al. [29] considered a series of individual Newtonian interactions interspersed with orbital evolution through GW emission. Mandel et al. [53] carried out analytical estimates of the hardening sequence to obtain the intermediate mass-ratio merger timescale. Leigh et al. [44] simulated the entire cluster with a mixture of analytical and numerical *N*-body analytical calculations, while MacLeod et al. [51] focused their *N*-body investigation on tidal disruptions of stars by the IMBH as well as merger events. We note that in the previous literature effects of pN terms are either not accounted for [44], or included only at the 2.5pN level [51, 73]. In this chapter we show a clear example in which lower order pN terms play a fundamental role in the dynamics. More specifically, an essential element that differs between the relativistic and non-relativistic dynamics turns out to be the 1pN precession of the periaapsis.

We introduce our numerical method and the simulation setup in Sect. 2.2. We describe our simulation results in Sect. 2.3. We discuss the results, including the detectability of GWs from intermediate mass-ratio coalescences, in Sect. 2.4.

2.2 Simulations

The *N*-body systems considered here consist of a massive particle, representing an IMBH, and two additional lower-mass species representing $10M_{\odot}$ compact remnants and $1M_{\odot}$ stars. Integrations of the *N*-body equations of motion were carried out using the direct summation *N*-body code phiGRAPEch [32]. This code incorporates Mikkola’s algorithmic chain regularization scheme including post-Newtonian terms of order 1pN, 2pN and 2.5pN (AR-CHAIN, [59]). Velocity dependent forces were included using the generalized midpoint method described by Mikkola and Merritt [58]. The algorithm produces exact trajectories for Newtonian two-body motion and regular results for strong encounters involving arbitrary numbers of bodies. Particles moving beyond the “chain radius” (r_{chain}) were advanced using a fourth-order integrator with forces computed on GPUs using the Sapporo library [25]. The chain particles were influenced by the global cluster dynamics through the particles in a perturber region, within a radius $r_{perturb}$ from the IMBH. phiGRAPEch is an ideal tool for the study of the dynamics of IMBHs in star clusters because it allows to study with extremely high precision the joint effect of 1pN, 2pN and 2.5pN terms and their interplay with Newtonian perturbations to the motion.

We performed 12 simulations all initialized as a King model with no primordial binaries, containing two mass species (BHs and stars) with a relative mass ratio of 10:1, and assuming that the total mass in BHs is 1% of the total cluster mass.

Finally, an initially stationary IMBH was placed at the center of the cluster. The analytical King model was chosen because, despite of their dynamical simplicity, they provide a good fit to observed surface brightness profiles. King models are defined as approximate iso-thermal spheres (where the velocity of a particle is largely independent of its position in the cluster) with a modified density profile such that the energy, as well as the number density, decreases with radius until it becomes zero at the tidal radius r_t . Together with the King radius

$$r_0 \equiv \sqrt{\frac{9\sigma^2}{4\pi G\rho_0}} \quad (2.1)$$

where σ is the velocity dispersion of the cluster and ρ_0 is its central density, this defines the concentration parameter $W_0 \equiv r_t/r_0$ ($W_0 = 7$ for all our simulations). The simulations were performed with number of particles $N \in \{32768, 65536\}$ IMBH mass, $M \in \{50, 100, 200\} M_\odot$ and cluster virial radius r_v defined as

$$\frac{M_{\text{tot}}^2}{r_v} \equiv \sum_{i=0}^N \sum_{j \neq i}^N \frac{m_i m_j}{|\vec{r}_i - \vec{r}_j|} \quad (2.2)$$

given cluster total mass M_{tot} , and particle masses and distances m and \vec{r} summed over all particle pairs i, j . r_v was in these simulations set as 3.5 pc which in turn gave $r_v \sim 5r_0$ for our choice of King models. For $N = 32768$ and all three IMBH masses, simulations with $r_v \in \{0.35, 1.0\}$ pc were also performed. The inclusion of high-order pN terms fixes the physical scale of the cluster, thus removing the conventional freedom for rescaling simulations in cluster size and density.

We observe the IMBH forming a binary with a BH within $\lesssim 20$ Myr in every simulated cluster. Only in one cluster ($N = 32768$, $M = 100M_\odot$, $r_v = 3.5$ pc) we observe a merger within the simulated time ($\simeq 100$ Myr), and in what follows we will focus on describing the detailed dynamics of this cluster. We acknowledge that as the main focus of this study is the dynamical formation and evolution of binaries, and higher order N -tuples, with the IMBH as the primary companion, all cluster particles are solely characterized by their mass and no stellar evolution is included in these simulations.

2.3 Results

The simulated globular cluster was initialised with the IMBH at rest at the center while the remaining stars and BHs follows a King model. Figure 2.1 shows the position of the IMBH and a subset of BH particles, and their subsequent movement within the cluster, relative to the center of mass of the entire cluster. This subset of the BH population were those that were ejected from the cluster during the simula-

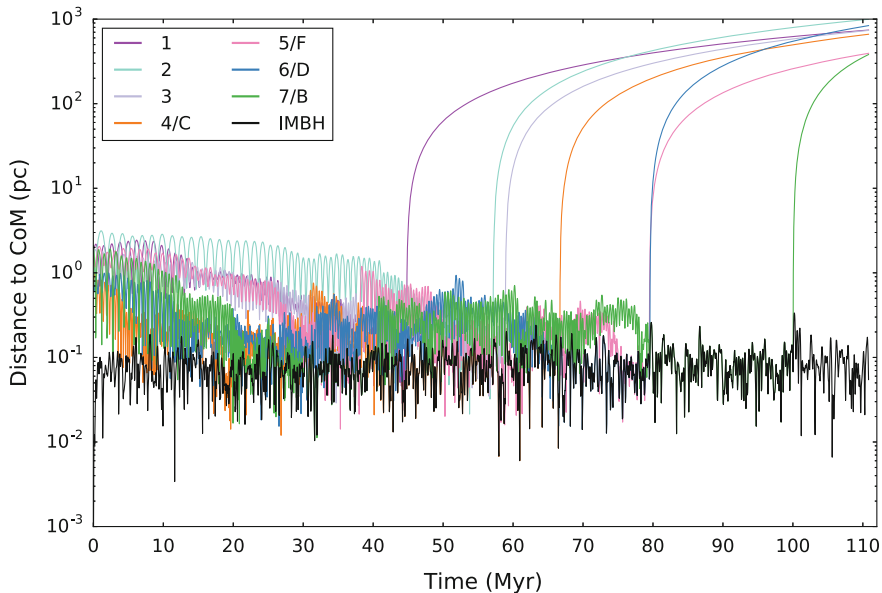


Fig. 2.1 Time evolution of the distance of the IMBH (in *black*) to the center of mass (CoM) of the entire cluster. Note how the IMBH is wandering throughout the simulation within a *central* region of extent $\lesssim 0.1$ pc around the cluster CoM. Also shown (in *colour*) are the BHs that were ejected from the cluster and the corresponding time of ejection. BHs for which we have assigned both a numerical and alphabetical index were bound to the IMBH before being ejected from the cluster. The evolution of the orbits of these BHs are also shown in Fig. 2.2

tion. Although the IMBH is initially at rest at the cluster center of mass, it quickly experiences significant Brownian motion within a sphere of radius ~ 0.1 pc around the center of mass. The typical distance wandered by the IMBH in the core is larger than the radius of influence of the IMBH.

Shifting the focus from the global dynamical behaviour within the cluster, Fig. 2.2 displays the time evolution of the relative distance to the IMBH of those BHs which experienced close encounters with the IMBH at some point of the simulation. In this figure we see that while the IMBH is interacting only weakly with its surroundings at the start of the simulation, after ~ 3 Myrs it forms a wide binary with a stellar particle, and after ~ 25 Myrs the binary companions are BHs, consistent with the expected mass segregation in this cluster. By comparing the ejected BHs between Figs. 2.1 and 2.2 it is clear that after the first few ejected BHs (which were driven by their initially relatively high kinetic energy and interactions with other cluster members) and following the formation of the IMBH-BH binary, all subsequent ejections are driven by interactions with the IMBH-BH binary. These interactions lead to the frequent substitution of the IMBH binary companion, with three out of the five observed substitution events leading to the former companion being ejected from the cluster. The remaining two were returned to the cluster BH population, where

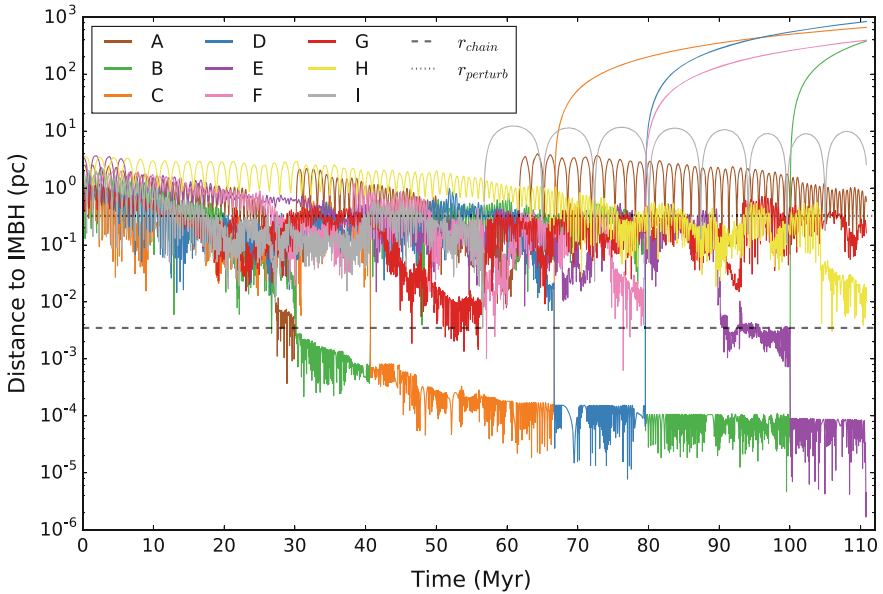


Fig. 2.2 Distance to the IMBH versus time for BHs which at any point in the simulation came within a sphere of 4 mpc around the IMBH. Within the first 3 Myrs the IMBH acquires a binary companion, at first a stellar particle which is quickly substituted for a BH companion at ~ 25 Myrs, in this case BH_A , forming a wide binary. Through interactions with other objects embedded in the cluster potential this binary is hardened. The IMBH–BH binary undergoes many companion substitutions, often while in hierarchical N -tuples, resulting in both later recaptures (BH_B) and ejections from the cluster ($\text{BH}_{C,D,B}$). The *dashed black line* marks the transition distance r_{chain} below which the dynamics are treated by AR-CHAIN under the gravitational influence of all perturbing particles within the region represented by the *dotted black line* (r_{perturb})

one BH (BH_B in Figs. 2.1 and 2.2) was later recaptured by the IMBH. Figure 2.2 also shows the transient 3-body interactions, such as the ejection of BH_F , and their effectiveness in the continued hardening of the IMBH–BH binary.

The time evolution of this binary is most clearly visualized in terms of its orbital parameters where Fig. 2.3 shows the IMBH–BH binary semi-major axis.¹ Once the IMBH captures a stellar-mass BH companion, the IMBH–BH binary is hardened by 3-body interactions. The hardening of the binary is clearly visible in Fig. 2.3 as the semi-major axis of the IMBH–BH binary decreases monotonically, with the jumps in semi-major axis being signs of energetic 3-body interactions. While Fig. 2.2 only shows the BH interactions, there are also a multitude of close encounters with stars carrying energy away from the IMBH–BH binary. The majority (~ 150) of these were ejected from the cluster, with moderate to high final velocities

¹The semi-major axes and eccentricities were computed using the post-Newtonian formalism given in Eq. (3.6) of Damour and Deruelle [21].

($v \lesssim 250 \text{ km s}^{-1}$), with the remainder being returned to the cluster stellar population distributing energy throughout the cluster.

The binary hardens through 3-body interactions on the typical timescale (e.g., [53, 72])

$$\tau_{\text{harden}} \simeq 10^8 \left(\frac{10 M_{\odot}}{m_*} \right) \left(\frac{v}{10 \text{ km s}^{-1}} \right) \left(\frac{10^{5.5} \text{ pc}^{-3}}{n} \right) \left(\frac{0.05 \text{ AU}}{a_i} \right) \text{ yr}, \quad (2.3)$$

where m_* is the interloper mass, v is the velocity dispersion in the cluster, n is the number density of stars and BHs in the cluster center, and a_i is the binary's semi-major axis.

As the binary hardens, after $\simeq 110 \text{ Myr}$, the time to the next interaction drops below the GW driven merger timescale which, in the limit of large binary eccentricities, is approximated by [68]

$$\tau_{\text{merge}} \simeq 3 \times 10^7 \left(\frac{10^5 M_{\odot}^3}{M^2 m} \right) \left(\frac{a_i}{0.05 \text{ AU}} \right)^4 (1 - e_i^2)^{7/2} \text{ yr}, \quad (2.4)$$

where e_i is the IMBH-BH binary eccentricity, M is the IMBH mass, and m is the mass of its BH companion. The semi-major axis a_{GW} at which the evolution of the binary eccentricity starts to be dominated by GW radiation, and no longer governed by 3-body interactions, can be found by setting

$$\tau_{\text{merge}} = (1 - e_i^2) \tau_{\text{harden}}. \quad (2.5)$$

where the factor of $(1 - e_i^2)$ comes from the fact that it is diffusion of angular momentum, and not energy, which initiates the GW dominated phase (c.f. Eq. 62 in [57]). This in turn gives

$$a_{\text{GW}} \simeq \frac{0.15}{\sqrt{1 - e_i^2}} \text{ AU}. \quad (2.6)$$

At separations below a_{GW} the evolution of the binary is dominated by energy loss due to GW emission. Mandel et al. [53] computed the total time to IMBH-BH coalescence by summing the hardening time to the last interaction with the subsequent merger timescale under the assumption that the last interaction is likely to leave the binary with an eccentricity of $\simeq 0.98$ [30]. However, as shown in what follows, even higher eccentricities can be reached during the complex 3-body interactions, possibly reducing the merger timescale [14, 73].

Figure 2.4 shows the evolution of the binary eccentricity where the inclination of outer to inner binary when the binary is part of a triple system (ι_0) is shown in Fig. 2.5. The complex dynamical structure of the surroundings of the binary, including both stellar and BH interactions, is evident in Fig. 2.4 where large amplitude variations of the IMBH-BH binary eccentricity are observed. The evolution of e_i and ι_0 is driven both by transient passes and by longer duration LK and post-Newtonian effects.

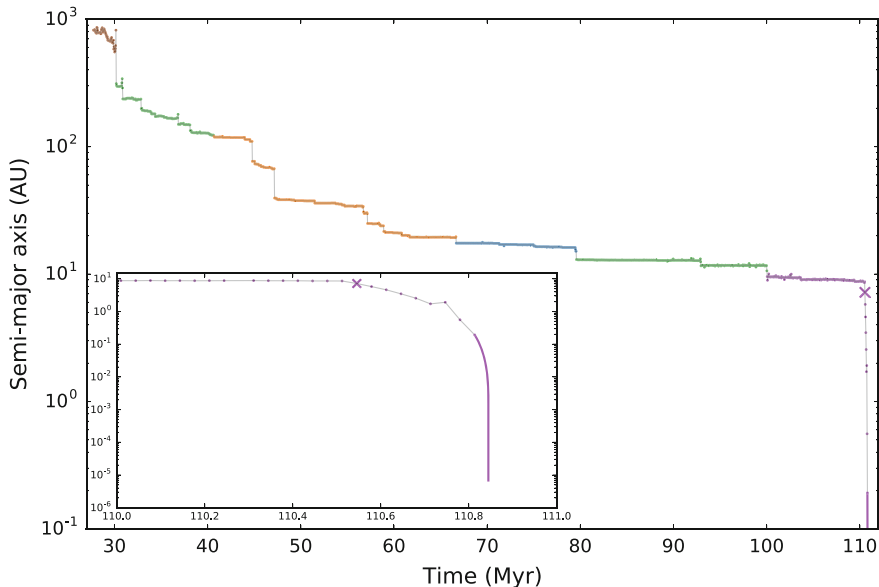


Fig. 2.3 A binary consisting of an IMBH and another BH will harden over time and lose energy to its surroundings, manifested by the shrinking of the binary’s semi-major axis. The colours match Fig. 2.2 to highlight the substitution of the binary companions. At the end of the simulation the IMBH, through external perturbation by BH_H , is set on a trajectory towards a merger with its binary companion BH_E while still inside the cluster. The point where GW emission becomes dominant in the orbital evolution (see Eq. 2.6) is marked by a purple \times . At the end of the simulation the binary orbit is evolved until merger according to Peters [68] marked by the solid purple line, this is further highlighted in the inset figure showing the last Myr of the binary before merger

The eccentricity oscillations in hierarchical triple systems can potentially drive up the eccentricity of the inner binary to very high values, possibly leading to faster GW driven mergers [1, 14, 62]. The timescale for a full oscillation in eccentricity is given as

$$T_{LK} \simeq \frac{P_i}{2\pi} \frac{M+m}{m_o} \left(\frac{a_o}{a_i} \right)^3 (1 - e_o^2)^{3/2} \quad (2.7)$$

where a_i, a_o are the semi-major axes of the inner and outer binary respectively (within the hierarchical triple system), e_o is the eccentricity of the outer orbit, m_o is the mass of the tertiary BH, and $P_i = 2\pi\sqrt{a_i^3/G(M+m)}$ is the orbital period of the inner binary [37]. We also define here a dimensionless angular momentum, as the angular momentum of the binary divided by the angular momentum of a circular orbit with the same semi-major axis: $\ell_i = \sqrt{1 - e_i^2}$; this is a useful quantity when discussing LK oscillations, as they do not affect the orbital energy. The timescale over which the inner binary changes the value of its angular momentum by order of itself is then [12, 17]

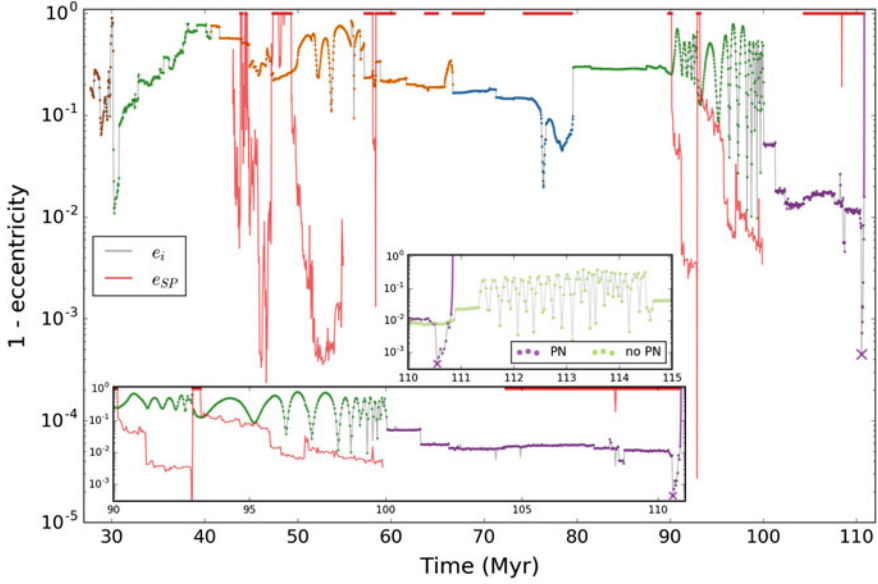


Fig. 2.4 Evolution of the IMBH-BH binary eccentricity. The colours of e_i match those of Fig. 2.2 to highlight the many substitutions of the binary companions. The figure shows clear evidence for both transient 3-body interactions as well as longer timescale LK oscillations. For the majority of the binary's presence in a hierarchical N -tuple LK effects are suppressed by the SP of the inner binary orbit. The precession is represented here as an effective eccentricity boundary e_{SP} above which LK oscillations are suppressed (corresponding to *below* the e_{SP} line in this figure). The *bottom* inset shows the last ~ 20 Myr exhibiting LK oscillations, bounded by e_{SP} , in a quadruple and later a triple BH system ended by the substitution of the IMBH binary companion. This last binary configuration is frozen at high e_i , suppressed by SP and later merged. The point where the binary evolution is dominated by GW emission is marked by a purple \times . At the end of the simulation the binary orbit is evolved using the formula of Peters [68] marked by the *solid purple line*. To further highlight the importance of the post-Newtonian dynamics the *upper* inset also includes a simulation (presented in *light green*) started at ~ 1 Myr before the observed merger, but using only Newtonian dynamics. This provides evidence for the importance of pN dynamics through the absence of the merger as well as the clear eccentricity oscillations in a triple system where SP would have provided complete LK suppression

$$\tau_{LK} \equiv \left| \frac{1}{\ell_i} \frac{d\ell_i}{dt} \right|_{LK}^{-1} \simeq T_{LK} \sqrt{1 - e_i^2} \quad (2.8)$$

directly related to the period of the LK oscillation.

At the quadrupole level of approximation and in the test particle limit, for an orbit librating around the argument of periapsis $\omega_i = \pi/2$ the maximum (ℓ_+) and minimum (ℓ_-) angular momenta during a LK cycle are related through the equation (e.g., [56])

$$\ell_+ \ell_- = \sqrt{\frac{5}{3}} \ell_z. \quad (2.9)$$

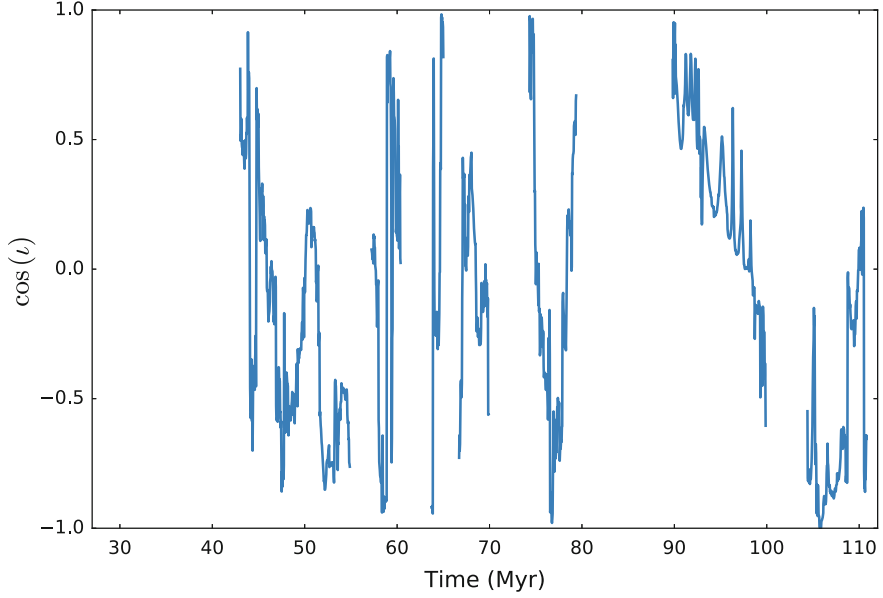


Fig. 2.5 Evolution of the inclination ι_0 between the inner (IMBH–BH binary) and outer orbits for the times when the IMBH exists in a bound triple system

In the previous expression $\ell_z = \ell_i \cos \iota_0$ is a conserved quantity for an initial orbital inclination ι_0 in the quadrupolar limit. From Eq. 2.9, and from the conservation of ℓ_z one finds that the maximum eccentricity that can be attained during a LK cycle is simply $e_{\max} = \sqrt{1 - (5/3) \cos^2 \iota_0}$ [39].

Post-Newtonian corrections to the orbital dynamics can affect the binary on similar timescales as τ_{LK} , where the most prominent effect would be the 1pN Schwarzschild precession (SP) of the argument of periapsis ω_i . To lowest order, the timescale associated with SP is

$$\tau_{SP} \equiv \left| \frac{1}{\pi} \frac{d\omega_i}{dt} \right|_{SP}^{-1} \simeq \frac{P_i}{6} \frac{a_i}{r_g} (1 - e_i^2) \quad (2.10)$$

with $r_g = G(M + m)/c^2$. When SP is considered, Eq. 2.9 becomes [13]:

$$\ell_+^2 \ell_-^2 = \frac{5}{3} \ell_z^2 + \frac{k}{3} \left(\frac{\ell_+ - \ell_-}{\ell_+^2 - \ell_-^2} \right) \ell_+ \ell_-, \quad (2.11)$$

with

$$k = 8 \frac{M}{m} \frac{r_g a_o^3}{a_i^4} (1 - e_o^2)^{3/2}. \quad (2.12)$$

This shows that SP effects can suppress the phase space available for libration for systems with $\tau_{SP} < \tau_{LK}$, reducing the maximum eccentricity attained during a LK cycle. In fact, from Eq. 2.11, given that the second term on the right hand side of the equation is always positive, we see that for a given ℓ_+ SP will lead to an increase of ℓ_- .

By setting $\tau_{LK} = \tau_{SP}$ we find the critical angular momentum

$$\ell_{SP} \sim \frac{r_g}{a_i} \frac{M+m}{m_o} \left(\frac{a_o}{a_i} \right)^3 \quad (2.13)$$

which in turn can be represented as an eccentricity boundary $e_{SP} = \sqrt{1 - \ell_{SP}^2}$ to the eccentricities within reach of LK oscillations. SP will dominate the orbital evolution of the inner binary at eccentricities larger than e_{SP} , thus quenching the possibility of eccentricity oscillations caused by LK resonance. When $\ell_{SP} \geq 1$, then SP will dominate over the torque from the outer tertiary BH for any value of e_i and LK oscillations are expected to be fully suppressed. In Fig. 2.4 we show when this happens using a solid red line at $\ell_{SP} = 1$. As expected, no LK oscillations occur when $\ell_{SP} \gtrsim 1$. In Fig. 2.4 the e_{SP} boundary is shown only when there is a hierarchical triple system present, with the IMBH-BH binary at its center. During the periods of active LK oscillations, for example between $\sim 90 - 100$ Myr, it is clear that the eccentricity of the IMBH-BH binary never exceeds the e_{SP} boundary. This is further evidence that SP plays a fundamental role in the dynamical evolution of the IMBH-BH binary in our simulations. The detailed interaction between LK and SP dynamical effects is also discussed by Naoz et al. [64] who find that, assuming Newtonian dynamics to octupolar order with an added 1pN (only) correction term, SP in hierarchical triples can excite eccentricity rather than suppress it for $\tau_{SP} \sim \tau_{LK}$. While qualitatively similar behaviour can be observed in our simulation, it is difficult to distinguish effects like this from other mechanisms subdominant to the LK oscillations (e.g., the hierarchical mass ratio configuration, stellar interlopers and the perturbing cluster potential) without further investigation.

In addition to LK suppression from relativistic precession, the presence of strong Newtonian precession, induced by the IMBH-BH binary existing within a dynamical cluster, would have similar effects on the binary orbital evolution. We find the classical precession to be negligible compared to SP for the periods when the IMBH-BH binary is in a hierarchical triple, and thus have no effect on the LK suppression caused by precession of the IMBH-BH orbit.

Between $\sim 90 - 93$ Myr we find that the IMBH-BH binary is part of a hierarchical quadruple BH (IMBH, BH_B, BH_E, BH_F), with a resolved two-level LK oscillation. As discussed by Hamers et al. [31], as the individual τ_{LK} for the two LK systems are comparable, this induces complex LK oscillations in the IMBH-BH binary, further enhancing the transfer of angular momentum away from it. This is most clearly exemplified by the eccentricity: the expected maximum eccentricity $e_{max} \simeq 0.3$ from $\iota_0 = 43.1^\circ$ at 90 Myr is substantially smaller than the eccentricities achieved during the existence of the quadruple BH. It is also interesting to note that the

two LK timescales associated with the quadruple are both below the corresponding τ_{SP} for the inner binary as well as the empirical timescale for the precession of ω_i induced by the presence of the quadruple within the stellar cluster. Eventually at $\simeq 93$ Myr the quadruple system is disrupted by the removal of the outermost BH. At $93 - 100$ Myr of evolution the eccentricity of the IMBH-BH binary clearly undergoes large-amplitude LK oscillations as expected given the high mutual inclination of the outer to inner orbit ($\iota_0 = 78.5^\circ$) at this time.

While the observed oscillations in eccentricity and inclination of the IMBH triple system show all signs of being caused by the LK mechanism, it is important to keep in mind that “pure” LK oscillations assume an isolated 3-body system. Here we are able to observe (for the first time) this mechanism acting on a triple system embedded in a dynamically evolving stellar cluster while also accounting for relativistic corrections to the motion.

Also interesting are the regions where $e_{SP} = 0$, or equivalently $\ell_{SP} \geq 1$. Here the SP is dominating the IMBH-BH binary to such a degree that no eccentricity oscillations driven by LK are possible. We find that the inclination of the IMBH-BH binary relative to the outer BH orbit evolves stochastically, attaining at times values near 40° which based on Eq. 2.9 should lead to LK eccentricity oscillations with a period $\simeq 5 \times 10^6$ years following Eq. 2.7.

Contrary to this, during the last ~ 10 Myr the IMBH-BH binary appears to be “frozen” at high e_i with SP suppressing any eccentricity reduction apart from the higher pN-order emission of GWs. After a strong interaction with a stellar interloper, which in turn is ejected from the cluster at $\sim 120 \text{ km s}^{-1}$, the loss of energy and angular momentum through GWs determines the ultimate fate of the binary, leading to its merger $\sim 300,000$ years later (see Fig. 2.6).

During the initial GW-dominated phase the binary experiences a small number of 3-body interactions with stellar interlopers, which are the cause of the “spikes” visible in Fig. 2.6. However, these interactions do not disrupt the binary inspiral.

A highly eccentric binary emits a broad spectrum of gravitational radiation during each periapsis passage. We identify the frequency of the harmonic containing the maximal gravitational radiation as [86]:

$$f_{\text{GW}} = \frac{\sqrt{G(M+m)}}{\pi} \frac{(1+e_i)^{1.1954}}{[a_i(1-e_i^2)]^{1.5}}; \quad (2.14)$$

this is the GW frequency plotted in Fig. 2.6.

The binary spends $\simeq 300,000$ years in the eLISA sensitive frequency window, which spans ($0.001 \text{ Hz} \lesssim f_{\text{GW}} \lesssim 1 \text{ Hz}$). Meanwhile, the last 6 s of the inspiral, followed by the merger and subsequent ringdown of the resulting IMBH, occur in the GW spectrum observable by Advanced LIGO ($f_{\text{GW}} \gtrsim 10 \text{ Hz}$). As suggested by Amaro-Seoane and Santamaría [11] for IMBH-IMBH binaries and Abbott et al. [4], Sesana [74] for binary BH systems similar to the detected GW150914 [5], this type of IMBH-BH coalescences represents a class of GW sources potentially observable in both space- and ground-based detectors, providing an opportunity for long-term

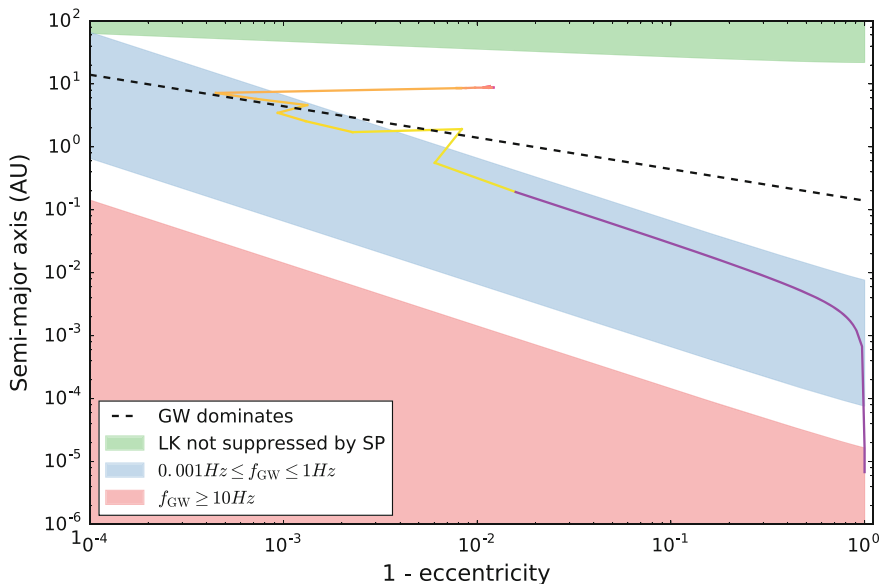


Fig. 2.6 As the IMBH–BH binary evolves during its final Myr (time increases from *red* to *yellow*) it is frozen at very high eccentricities due to the suppression of LK oscillations by the SP of the IMBH–BH binary. The *red* region indicates where this suppression would be absent. The presence of a stable triple system, as indicated in Fig. 2.2, causes perturbations of the IMBH orbit from both the tertiary BH_H and additional stellar interlopers. One of the stellar perturbations bring the three objects so close together that the IMBH–BH binary orbital evolution becomes dominated by emission of GWs. Additionally, this ejects the stellar interloper at a velocity $\sim 120 \text{ km s}^{-1}$. GW emission dominates below the *dashed black line*, given by Eq. 2.6; in this regime merger through the emission of GWs will occur before the next 3-body interaction can significantly alter the IMBH–BH binary eccentricity, and thus its evolutionary timescale (c.f. the interloper which initiated the merger trajectory). Much of the GW dominated evolution occurs at GW frequencies observable by eLISA, as indicated by the *blue* region. As the IMBH–BH binary evolves along its merger trajectory there are still a small number of minor three body encounters with stellar interlopers passing within a few semi-major axes of the binary CoM; these interactions are the cause of the “spikes” visible in the merger trajectory. These interactions are consistent with the timescales given in Eqs. 2.3 and 2.4, which predict that the last interaction before merger should occur when this system has a semi-major axis of $\sim 1 \text{ AU}$. At the end of the simulation the binary’s orbit is evolved to merger, within the Advanced LIGO sensitive band (marked by the *green* region), according to Peters [68], as shown by the *purple line*

detailed studies of both their formation environments and probes of general relativity itself. We discuss the near-term prospects of detecting such binary mergers with Advanced LIGO in the following section.

To further verify the importance of the inclusion of the pN effects in our models, the simulation was restarted $\sim 1 \text{ Myr}$ before the merger, removing all pN terms from the equations of motion. As shown by the light green samples in the upper inset of Fig. 2.4, removing pN terms results in eccentricity oscillations without, of course, a GW induced merger. During these oscillations the IMBH remains in a bound triple

system (IMBH, BH_E , BH_H) in which SP would have been the dominant dynamical factor, completely removing the possibility for LK oscillations.

In addition, we performed one simulation, also started ~ 1 Myr before the merger, where the chain regularization was disabled. In this simulation the surrounding N -body integrator could not accurately follow the very hard IMBH-BH binary; this had the effect of significantly slowing down the simulation while no longer adhering to the conservation of total energy within the cluster. This loss of $\frac{\Delta E}{E} \sim 0.01$ per time-step $\Delta t = 67\text{kyr}$ accumulates as the simulation progresses, to be compared with $\frac{\Delta E}{E} \sim 10^{-4}$ per time-step when including the chain regularization. These results further demonstrate the importance of using a high accuracy integrator like ARCHAIN in order to study the evolution of IMBHs in cluster simulations.

2.4 Discussion

Gravitational waves from intermediate mass-ratio coalescences are observable with both a future space-based GW detector [23] and the advanced network of ground-based detectors [8, 33]. The SP-induced freezing of the IMBH-BH orbit at high eccentricities will be conducive for the production of a merging binary, as efficient GW emission is then possible for larger binary semi-major axes as compared to a circular system [68, 75]. The observed binary inspiral is in the eLISA sensitivity band throughout the circularizing phase. However, detection and parameter estimation at very high eccentricities could prove problematic without high-accuracy eccentric templates for matched filtering the bursts of radiation expected during the few periastris passages over the lifetime of a space-borne mission [10, 16, 40, 71]. Both detection and parameter estimation would be more amenable to existing techniques later in the orbital evolution [38, 63, 65, 77, 80], for $e_i \lesssim 0.1$ in Fig. 2.6, and with only ten years from $e_i = 0.1$ until merger for this system a co-observing campaign together with ground-based detectors, where the system is effectively fully circularized, would be possible.

As discussed by Sesana [74] and Vitale [85] in relation to binary BHs similar to GW150914, the extended observation in eLISA would provide excellent constraints on the binary masses, sky position and coalescence time with the observational gap of $1\text{Hz} \leq f_{\text{GW}} \leq 10\text{Hz}$ between eLISA and Advanced LIGO only spanning ~ 1 h. Note that the exact observational gap depends on the distance to the source, corresponding to its observed signal-to-noise ratio, and therefore determining the frequency band where the signal will be below the detector noise floor. This advance information would however allow for optimization of the ground-based detector network, both in terms of active tuning of the detector sensitivity, operational scheduling and the analysis pipelines, as well as pre-pointing of electromagnetic follow-up telescopes.² For the remainder of this section we will focus on detectability and rates for ground-

²No electromagnetic counterpart is expected from the merger of an IMBH-BH binary in the standard scenario (e.g., [49]), but see Connaughton et al. [20].

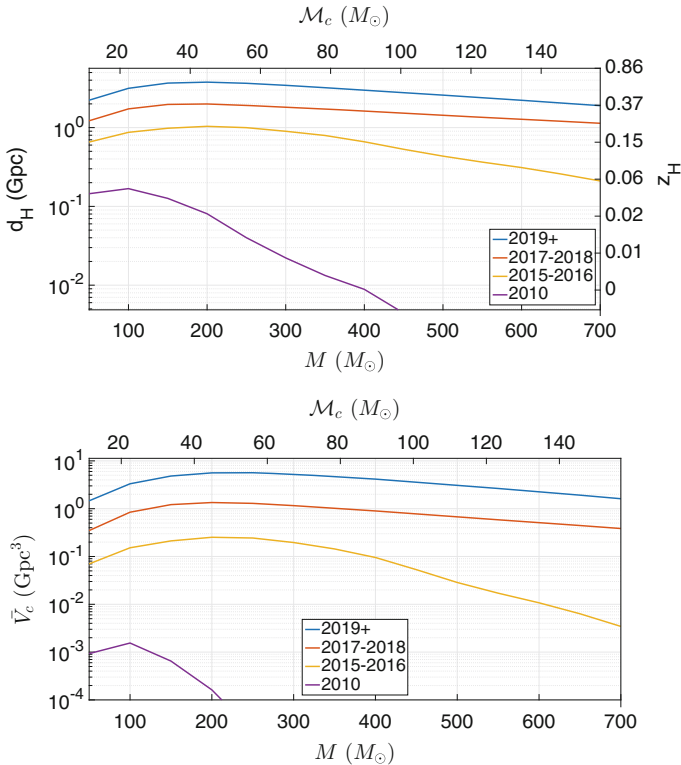


Fig. 2.7 *Top* Horizon distance (left axis) and horizon redshift (right axis) as a function of IMBH mass for IMBH–BH coalescences with non-spinning components with a 10:1 mass ratio, for different detector sensitivities (see text). *Bottom* Detection-weighted sensitive comoving volume, Eq. 2.15; when multiplied by a constant merger rate per unit comoving volume per unit source time, this yields a detection rate

based detectors alone, primarily motivated by the lack of a space-based detector for at least the next decade.

In Fig. 2.7 we show the sensitivity of a network of ground-based detectors to GWs from an IMBH–BH coalescence with non-spinning components with a mass ratio of 10:1, as a function of IMBH mass.

The top panel of Fig. 2.7 shows the horizon distance d_H , which is the luminosity distance at which GWs from a face-on overhead binary would be detected at a signal-to-noise ratio of 8 by a single detector with the sensitivity of Advanced LIGO; the corresponding horizon redshift z_H is shown on the right vertical axis. This signal-to-noise ratio is used as an approximation for sensitivity by the full network [3, 6]; the actual sensitivity depends on the network configuration, data quality, and signal duration. We use the noise power spectral density (PSD) of H1 (the LIGO detector in Hanford, WA) during the S6 science run (curve labeled ‘2010’, [47]), the measured noise PSD of H1 during the 2015 observing run O1 (‘2015–2016’, [48]),

low-end predictions for Advanced LIGO noise PSD for the later stages of detector commissioning (‘2017–2018’, O3 configuration of [7]), and for design sensitivity runs in the zero detuning, high laser power configuration (‘2019+’, [46]). We use circular effective one-body waveforms calibrated to numerical relativity for signal-to-noise-ratio calculations [79].

The bottom panel of Fig. 2.7 shows the surveyed detection-weighted comoving volume \bar{V}_c

$$\bar{V}_c = \int_0^\infty \frac{dV_c}{dz} f_d(z) \frac{1}{1+z} dz, \quad (2.15)$$

where $\frac{dV_c}{dz}$ is computed using the Planck [19] cosmology, $f_d(z)$ is the probability that a binary with the given source-frame masses at redshift z is louder than the signal-to-noise ratio threshold of 8 (integrated over isotropically distributed sky locations and orientations), and the last factor corrects for the difference in source and observer clocks. With this definition, $\mathcal{R}\bar{V}_c T$ yields the expected number of detections during an observing run with (at least double-coincident) duration T assuming a constant merger rate \mathcal{R} per unit comoving volume per unit source time.

Intermediate mass-ratio coalescences can be observed to a horizon distance of ~ 1 Gpc during the O1 science run, and a horizon redshift $z \sim 0.6$ at full design sensitivity. Figure 2.7 assumes a 10:1 mass ratio. It can be roughly rescaled to other mass ratios by noting that, for a fixed IMBH mass, the signal-to-noise ratio at a given distance, and hence the horizon distance, will scale as $\sqrt{m/M}$ when the signal is inspiral-dominated, and as m/M when the signal is ringdown-dominated. The transition between the two regimes occurs at $M + m \sim 200 M_\odot$ at Advanced LIGO design sensitivity (see Fig. 9 of [35], which also discusses inference on the parameters of coalescences of intermediate mass-ratio binaries). As a comparison, if the BHs in GW150914 (both BHs in the initial binary and the merger product) had been the lower mass member of a 10:1 mass ratio IMBH–BH binary, all signals would be ringdown-dominated [5]. The same is valid for the marginally astrophysically significant event LVT151012 [6] where only the lower mass BH from the initial binary would produce an inspiral-dominated signal.

The IMBH–BH coalescence rate is highly uncertain. Our simulations suggest that around one IMBH–BH merger per ten globular clusters is probable in the first \sim hundred million years of the lifetime of a cluster hosting a suitable IMBH. The merger product may well be ejected from the cluster by the recoil kick from asymmetric GW emission in the last few pre-merger orbits. Assuming the IMBH is not spinning, the kick velocity for a 10:1 mass ratio coalescence is $\simeq 60 \text{ km s}^{-1}$ [27], comparable to the typical $\sim 50 \text{ km s}^{-1}$ escape velocity from a globular cluster. If so, at most \sim one IMBH–BH merger would happen per cluster before the IMBH is ejected.

The remaining 11 simulations followed a similar initial dynamical evolution to the cluster discussed in detail in this chapter, with all IMBHs forming a binary with a BH within $\lesssim 20 \text{ Myr}$. These binaries are hardened by 3-body interactions and at the final time of the simulation the binaries had estimated $\tau_{\text{merge}} \sim$ Hubble time. These estimates do not take into account either further 3-body interactions, SP or LK effects and should be seen as upper limits for a time to merger from

GW emission. It should however be noted that in two of the clusters with small r_v ($r_v = 0.35\text{pc}$, $M = (50, 100)M_\odot$) the IMBH–BH binary underwent periods of rapid 3-body interactions which led to the ejection of the IMBH–BH binary (without disrupting it) from the cluster.

Even if the merger product is retained, there is a trivial upper limit on the number of mergers per cluster in the Advanced LIGO sensitive frequency band. By the time the IMBH grows beyond several hundred solar masses (see Fig. 2.7), the sensitivity drops significantly; hence, only ~ 30 IMBH–BH per cluster are observable.

Therefore, the IMBH–BH coalescence rate per suitable cluster may vary between 1 and 30 mergers over the cluster’s ~ 10 Gyr lifetime, or $0.1\text{--}3$ mergers Gyr^{-1} . The space density of globular clusters is $\sim 3 \text{ Mpc}^{-3}$ [70]. Following Mandel et al. [53], we will parametrize the fraction of suitable globular clusters (those with the right IMBH mass and central density) by f . Then the total merger rate is in the range $R \in [0.03(f/0.1), (f/0.1)] \text{ Gpc}^{-3} \text{ yr}^{-1}$. Multiplying this by the surveyed detection-weighted comoving volume, we may expect $\sim 0.1\text{--}5 \times (f/0.1)$ detections per year at full sensitivity. In the near term, $0.01\text{--}1 \times (f/0.1)$ detections may be possible during the upcoming O2 6-month observing run, assuming a $\sim 50\%$ coincident duty cycle.³

This calculation may well be optimistic. It assumed a constant merger rate over the cluster lifetime; however, most local globular clusters are old (e.g., [43]), and mergers are in general more likely early in the cluster lifetime.⁴ Therefore, most mergers may happen at high redshift, where they are unlikely to be detectable. Finally, the fiducial choice $f = 0.1$ is fairly arbitrary; much lower values, including $f = 0$, are possible. On the other hand, if IMBHs are spinning, prograde inspirals could yield higher signal-to-noise ratios, and the detection volume and rate would increase even after averaging over isotropic inspiral orbits [52].

We have also looked for evidence of possible tidal disruptions of stars by the IMBH (see [51], for a recent analysis). Our problem set up is not ideal for this investigation, since we have only two stellar types in addition to the IMBH: one solar mass “stars” and ten solar mass “black holes”. None of the one-solar-mass stars in our simulation approach the IMBH within the tidal disruption radius. However, if we consider the black holes as proxies for evolving stars, we find that a few would approach within the IMBH tidal disruption radius while in the giant phase of their evolution. Given the gradual hardening of the innermost binary, it is likely that the nominal tidal disruption radius would be reached through stellar evolution rather than a dynamically-driven encounter. Hence, rather than transient tidal disruptions, we may expect to see Roche lobe overflows, perhaps leading to ultraluminous X-ray binaries such as ESO 243-49 HLX-1 [24, 26]. In the case of stellar companions additional sources of apsidal

³These rates should be considered in relation to the upper limits on the rate of binary IMBH coalescences from LIGO–Virgo observations, which are $\geq \mathcal{O}(10^3)$ higher depending on the IMBH masses considered [2].

⁴Keep in mind the non-mergers observed in the 11 simulations performed in preparation for this chapter, but also the fact that each eventual merger carries a non-negligible probability of ejection of the IMBH.

precession (for example, precession due to tidal and rotational bulges) may arise and quench LK oscillations similarly to SP as discussed above.

The capability of our simulation tracking both the complex dynamical features and the merger stands in contrast with previous work such as Leigh et al. [44], who did not include any pN effects and were thus unable to observe the quenching of LK oscillations due to SP. This could lead to the production of IMBH-BH binaries with artificially long lifetimes as they were unable to merge by the emission of GWs. This issue was partly addressed by MacLeod et al. [51], who included GW mergers following Peters [68]; however, the interplay of LK effects with SP (and tides in the case of stellar companions) would likely affect their merger rate estimates. Finally, neither the N -body simulations in Leigh et al. [44], MacLeod et al. [51] nor in this work included any population of primordial binaries (but see [36, 82, 83]), and while binaries which does not include the IMBH can form these would not be specifically tracked. The presence of primordial binary BHs in combination with an IMBH has been shown to affect the retention of BHs in the cluster as well as the evolution of the fraction of BHs in binaries [44, 69, 83], and would thus require a more careful treatment in future studies.

2.5 Conclusion

We have, in a simulation, observed a merger of a $100M_{\odot}$ IMBH and a $10M_{\odot}$ BH within a globular cluster as part of the first simulation campaign accounting for post-Newtonian dynamics in the region around the IMBH. This has provided insight into the competitive interplay between pN effects and LK eccentricity oscillations in hierarchical systems as a mechanism for producing and hardening an IMBH–BH binary. We have observed suppression of LK oscillations caused by the pN Schwarzschild precession of the IMBH–BH binary giving clear evidence for the necessity of including pN dynamics in future simulations of globular clusters to fully capture all relevant dynamical effects leading to the formation, evolution and merger of an IMBH–BH binary. This is especially relevant at the end of our simulation, where fast relativistic precession of the IMBH–BH binary freezes its orbit at high eccentricities, thus facilitating the onset of an inspiraling trajectory towards a merger.

Future extensions to this work will include a larger spectrum of masses (both for the IMBH and the surrounding cluster particles), longer simulation times (requiring further optimization of the code) and additional physical effects (e.g., stellar evolution models, population of primordial binaries and external tidal fields). We have also commented on the detectability of gravitational waves emitted from an IMBH–BH merger by both space-based and ground-based observatories, with a possible detection within the next decade.

References

1. Aarseth, S. J. (2012). Mergers and ejections of black holes in globular clusters. *Monthly Notices of the Royal Astronomical Society*, 422, 841–848. [arXiv:1202.4688](#).
2. Aasi, J., Abbott, B. P., Abbott, R., Abbott, T., Abernathy, M. R., Accadia, T., et al. (2014). Search for gravitational radiation from intermediate mass black hole binaries in data from the second LIGO-Virgo joint science run. *Physical Review D*, 89(12), 122003. [arXiv:1404.2199](#).
3. Abadie, J., et al. (2010). Predictions for the rates of compact binary coalescences observable by ground-based gravitational-wave detectors. *Classical and Quantum Gravity*, 27, 173001.
4. Abbott, B. P., Abbott, R., Abbott, T. D., Abernathy, M. R., Acernese, F., Ackley, K., Adams, C., Adams, T., Addesso, P., Adhikari, R. X., et al. (2016a). Astrophysical implications of the binary black-hole merger GW150914. *Astrophysical Journal*, 818, L22. [arXiv:1602.03846](#).
5. Abbott, B. P., Abbott, R., Abbott, T. D., Abernathy, M. R., Acernese, F., Ackley, K., Adams, C., Adams, T., Addesso, P., Adhikari, R. X., et al. (2016b). Observation of gravitational waves from a binary black hole merger. *Physical Review Letters*, 116(6), 061102. [arXiv:1602.03837](#).
6. Abbott, B. P., Abbott, R., Abbott, T. D., Abernathy, M. R., Acernese, F., Ackley, K., et al. (2016c). The Rate of binary black hole mergers inferred from advanced LIGO observations surrounding GW150914. arXiv e-prints [arXiv:1602.03842](#).
7. Abbott, B. P., et al. (2016). Prospects for observing and localizing gravitational-wave transients with advanced LIGO and advanced virgo. *Living Reviews in Relativity*, 19(1). [arXiv:1304.0670](#).
8. Acernese, F., Alshourbagy, M., Antonucci, F., et al. (2009). Advanced virgo baseline design. Virgo Technical Report VIR-0027A-09.
9. Amaro-Seoane, P., & Freitag, M. (2006). Intermediate-mass black holes in colliding clusters: Implications for lower frequency gravitational-wave astronomy. *Astrophysical Journal*, 653, L53–L56. [arXiv:astro-ph/0610478](#).
10. Amaro-Seoane, P., Gair, J. R., Freitag, M., Miller, M. C., Mandel, I., Cutler, C. J., et al. (2007). Topical review: intermediate and extreme mass-ratio inspirals-astronomy, science applications and detection using LISA. *Classical and Quantum Gravity*, 24, R113–R169. [arXiv:astro-ph/0703495](#).
11. Amaro-Seoane, P., & Santamaría, L. (2010). Detection of IMBHs with ground-based gravitational wave observatories: a biography of a binary of black holes, from birth to death. *Astrophysical Journal*, 722, 1197–1206. [arXiv:0910.0254](#).
12. Antonini, F., Chatterjee, S., Rodriguez, C. L., Morscher, M., Pattabiraman, B., Kalogera, V., & Rasio, F. A. (2016a). Black hole mergers and blue stragglers from hierarchical triples formed in globular clusters. *Astrophysical Journal*, 816, 65. [arXiv:1509.05080](#).
13. Antonini, F., Hamers, A. S., & Lithwick, Y. (2016b). Dynamical constraints on the origin of hot and warm Jupiters with close friends. arXiv e-prints [arXiv:1604.01781](#).
14. Antonini, F., Murray, N., & Mikkola, S. (2014). Black hole triple dynamics: a breakdown of the orbit average approximation and implications for gravitational wave detections. *Astrophysical Journal*, 781, 45. [arXiv:1308.3674](#).
15. Berghea, C. T., Weaver, K. A., Colbert, E. J. M., & Roberts, T. P. (2008). Testing the paradigm that ultraluminous x-ray sources as a class represent accreting intermediate-mass black holes. *Astrophysical Journal*, 687, 471–487. [arXiv:0807.1547](#).
16. Berry, C. P. L., & Gair, J. R. (2013). Observing the Galaxy’s massive black hole with gravitational wave bursts. *MNRAS*, 429, 589–612. [arXiv:1210.2778](#).
17. Bode, J. N., & Wegg, C. (2014). Production of EMRIs in supermassive black hole binaries. *MNRAS*, 438, 573–589.
18. Brown, D. A., Brink, J., Fang, H., Gair, J. R., Li, C., Lovelace, G., Mandel, I., & Thorne, K. S. (2007). Prospects for detection of gravitational waves from intermediate-mass-ratio inspirals. *Physical Review Letters*, 99(20), 201102. [arXiv:gr-qc/0612060](#).
19. Collaboration, P., Ade, P. A. R., Aghanim, N., Arnaud, M., Ashdown, M., Aumont, J., et al. (2015). Planck 2015 results. *XIII Cosmological parameters*. arXiv e-prints [arXiv:1502.01589](#).

20. Connaughton, V., Burns, E., Goldstein, A., Briggs, M. S., Zhang, B.-B., Hui, C. M., et al. (2016). Fermi GBM observations of LIGO gravitational wave event GW150914. *arXiv e-prints* [arXiv:1602.03920](#).
21. Damour, T., & Deruelle, N. (1985). General relativistic celestial mechanics of binary systems. I. The post-Newtonian motion. *Annales de l'IHP Physique Théorique*, 43(1), 107–132, 43, 107–132.
22. Davis, S. W., Narayan, R., Zhu, Y., Barret, D., Farrell, S. A., Godet, O., et al. (2011). The cool accretion disk in ESO 243–49 HLX-1: further evidence of an intermediate-mass black hole. *Astrophysical Journal*, 734, 111. [arXiv:1104.2614](#).
23. eLISA Consortium. (2013). The gravitational universe. *arXiv e-prints* [arXiv:1305.5720](#).
24. Farrell, S. A., Webb, N. A., Barret, D., Godet, O., & Rodrigues, J. M. (2009). An intermediate-mass black hole of over 500 solar masses in the galaxy ESO243-49. *Nature*, 460, 73–75.
25. Gaburov, E., Harfst, S., & Portegies Zwart, S. (2009). SAPPORO: A way to turn your graphics cards into a GRAPE-6. *New Astronomy*, 14, 630–637. [arXiv:0902.4463](#).
26. Godet, O., Lombardi, J. C., Antonini, F., Barret, D., Webb, N. A., Vingless, J., et al. (2014). Implications of the delayed 2013 outburst of ESO 243–49 HLX-1. *Astrophysical Journal*, 793, 105. [arXiv:1408.1819](#).
27. González, J. A., Sperhake, U., Brüggmann, B., Hannam, M., & Husa, S. (2007). Maximum kick from nonspinning black-hole binary inspiral. *Physical Review Letters*, 98(9), 091101. [arXiv:gr-qc/0610154](#).
28. Graham, A. W., & Scott, N. (2013). The M_{BH} - $L_{spheroid}$ relation at high and low masses, the quadratic growth of black holes, and intermediate-mass black hole candidates. *Astrophysical Journal*, 764, 151. [arXiv:1211.3199](#).
29. Gültekin, K., Miller, M. C., & Hamilton, D. P. (2004). Growth of intermediate-mass black holes in globular clusters. *Astrophysical Journal*, 616, 221–230. [arXiv:astro-ph/0402532](#).
30. Gültekin, K., Miller, M. C., & Hamilton, D. P. (2006). Three-body dynamics with gravitational wave emission. *Astrophysical Journal*, 640, 156–166. [arXiv:astro-ph/0509885](#).
31. Hamers, A. S., Perets, H. B., Antonini, F., & Portegies Zwart, S. F. (2015). Secular dynamics of hierarchical quadruple systems: the case of a triple system orbited by a fourth body. *MNRAS*, 449, 4221–4245. [arXiv:1412.3115](#).
32. Harfst, S., Gualandris, A., Merritt, D., & Mikkola, S. (2008). A hybrid N-body code incorporating algorithmic regularization and post-Newtonian forces. *MNRAS*, 389, 2–12. [arXiv:0803.2310](#).
33. Harry, G. M., & The LIGO Scientific Collaboration. (2010). Advanced LIGO: the next generation of gravitational wave detectors. *Classical and Quantum Gravity*, 27(8), 084006. [arXiv:1103.2728](#).
34. Haster, C.-J., Antonini, F., Kalogera, V., & Mandel, I. (2016a). N-body dynamics of intermediate mass-ratio inspirals. (In preparation).
35. Haster, C.-J., Wang, Z., Berry, C. P. L., Stevenson, S., Veitch, J., & Mandel, I. (2016b). Inference on gravitational waves from coalescences of stellar-mass compact objects and intermediate-mass black holes. *MNRAS*, 457, 4499–4506. [arXiv:1511.01431](#).
36. Heggie, D. C., Trenti, M., & Hut, P. (2006). Star clusters with primordial binaries—I. Dynamical evolution of isolated models. *MNRAS*, 368, 677–689. [arXiv:astro-ph/0602408](#).
37. Holman, M., Touma, J., & Tremaine, S. (1997). Chaotic variations in the eccentricity of the planet orbiting 16 Cygni B. *Nature*, 386, 254–256.
38. Huerta, E. A., Kumar, P., McWilliams, S. T., O’Shaughnessy, R., & Yunes, N. (2014). Accurate and efficient waveforms for compact binaries on eccentric orbits. *Physical Review D*, 90(8), 084016. [arXiv:1408.3406](#).
39. Innanen, K. A., Zheng, J. Q., Mikkola, S., & Valtonen, M. J. (1997). The Kozai Mechanism and the stability of planetary orbits in binary star systems. *Astronomical Journal*, 113, 1915.
40. Key, J. S., & Cornish, N. J. (2011). Characterizing spinning black hole binaries in eccentric orbits with LISA. *Physical Review D*, 83(8), 083001. [arXiv:1006.3759](#).
41. Konstantinidis, S., Amaro-Seoane, P., & Kokkotas, K. D. (2013). Investigating the retention of intermediate-mass black holes in star clusters using N-body simulations. *Astronomy & Astrophysics*, 557, A135. [arXiv:1108.5175](#).

42. Kozai, Y. (1962). Secular perturbations of asteroids with high inclination and eccentricity. *Astronomical Journal*, 67, 591.
43. Kruijssen, J. M. D. (2012). On the fraction of star formation occurring in bound stellar clusters. *MNRAS*, 426, 3008–3040. [arXiv:1208.2963](#).
44. Leigh, N. W. C., Lützgendorf, N., Geller, A. M., Maccarone, T. J., Heinke, C., & Sesana, A. (2014). On the coexistence of stellar-mass and intermediate-mass black holes in globular clusters. *MNRAS*, 444, 29–42. [arXiv:1407.4459](#).
45. Lidov, M. L. (1962). The evolution of orbits of artificial satellites of planets under the action of gravitational perturbations of external bodies. *Planetary and Space Science*, 9, 719–759.
46. LIGO Scientific Collaboration (2010a). Advanced LIGO anticipated sensitivity curves. <https://dcc.ligo.org/cgi-bin/DocDB/ShowDocument?docid=2974>.
47. LIGO Scientific Collaboration (2010b). H1 Sensitivity. http://labcit.ligo.caltech.edu/~jzweizig/distribution/LSC_Data/S6/.
48. LIGO Scientific Collaboration (2015). H1 Calibrated Sensitivity Spectra Oct 1 2015 (Representative for Start of O1). Document number G1501223-v3. <https://dcc.ligo.org/LIGO-G1501223/public>.
49. Lyutikov, M. (2016). Fermi GBM signal contemporaneous with GW150914 - an unlikely association. arXiv e-prints [arXiv:1602.07352](#).
50. Maccarone, T. J., & Servillat, M. (2008). Radio observations of NGC 2808 and other globular clusters: constraints on intermediate-mass black holes. *MNRAS*, 389, 379–384. [arXiv:0806.2387](#).
51. MacLeod, M., Trenti, M., & Ramirez-Ruiz, E. (2016). The close stellar companions to intermediate-mass black holes. *Astrophysical Journal*, 819, 70. [arXiv:1508.07000](#).
52. Mandel, I. (2007). Spin distribution following minor mergers and the effect of spin on the detection range for low-mass-ratio inspirals. arXiv e-prints [arXiv:0707.0711](#).
53. Mandel, I., Brown, D. A., Gair, J. R., & Miller, M. C. (2008). Rates and characteristics of intermediate mass ratio inspirals detectable by advanced LIGO. *Astrophysical Journal*, 681, 1431–1447. [arXiv:0705.0285](#).
54. Mapelli, M. (2016). Massive black hole binaries from runaway collisions: the impact of metallicity. *MNRAS*. [arXiv:1604.03559](#).
55. Mapelli, M., Huwyler, C., Mayer, L., Jetzer, P., & Vecchio, A. (2010). Gravitational waves from intermediate-mass black holes in young clusters. *Astrophysical Journal*, 719, 987–995. [arXiv:1006.1664](#).
56. Merritt, D. (2013). *Dynamics and evolution of galactic nuclei*.
57. Merritt, D., Alexander, T., Mikkola, S., & Will, C. M. (2011). Stellar dynamics of extreme-mass-ratio inspirals. *Physical Review D*, 84(4), 044024. [arXiv:1102.3180](#).
58. Mikkola, S., & Merritt, D. (2006). Algorithmic regularization with velocity-dependent forces. *MNRAS*, 372, 219–223. [arXiv:astro-ph/0605054](#).
59. Mikkola, S., & Merritt, D. (2008). Implementing few-body algorithmic regularization with post-newtonian terms. *Astronomical Journal*, 135, 2398–2405. [arXiv:0709.3367](#).
60. Miller, M. C. (2002). Gravitational radiation from intermediate-mass black holes. *Astrophysical Journal*, 581, 438–450. [arXiv:astro-ph/0206404](#).
61. Miller, M. C., & Colbert, E. J. M. (2004). Intermediate-mass black holes. *International Journal of Modern Physics D*, 13, 1–64. [arXiv:astro-ph/0308402](#).
62. Miller, M. C., & Hamilton, D. P. (2002). Production of intermediate-mass black holes in globular clusters. *MNRAS*, 330, 232–240. [arXiv:astro-ph/0106188](#).
63. Moore, B., Favata, M., Arun, K. G., & Kant Mishra, C. (2016). Gravitational-wave phasing for low-eccentricity inspiralling compact binaries to 3PN order. arXiv e-prints [arXiv:1605.00304](#).
64. Naoz, S., Kocsis, B., Loeb, A., & Yunes, N. (2013). Resonant post-newtonian eccentricity excitation in hierarchical three-body systems. *Astrophysical Journal*, 773, 187. [arXiv:1206.4316](#).
65. Nishizawa, A., Berti, E., Klein, A., & Sesana, A. (2016). eLISA eccentricity measurements as tracers of binary black hole formation. arXiv e-prints [arXiv:1605.01341](#).
66. Pasham, D. R., Strohmayer, T. E., & Mushotzky, R. F. (2015). A 400 solar mass black hole in the Ultraluminous X-ray source M82 X-1 accreting close to its Eddington limit. *Nature*, 513(7516), 74–76. [arXiv:1501.03180](#)

67. Pasquato, M., Miocchi, P., Sohn, B. W., & Lee, Y.-W. (2016). Globular clusters hosting intermediate-mass black-holes: no mass-segregation based candidates. *arXiv e-prints* [arXiv:1604.03554](#).
68. Peters, P. C. (1964). Gravitational radiation and the motion of two point masses. *Physical Review*, 136, 1224–1232.
69. Pfahl, E. (2005). Binary disruption by massive black holes in globular clusters. *Astrophysical Journal*, 626, 849–852. [arXiv:astro-ph/0501326](#).
70. Portegies Zwart, S. F., & McMillan, S. L. W. (2000). Black hole mergers in the universe. *Astrophysical Journal*, 528, L17.
71. Porter, E. K., & Sesana, A. (2010). Eccentric massive black hole binaries in LISA I: The detection capabilities of circular templates. *arXiv e-prints* [arXiv:1005.5296](#).
72. Quinlan, G. D. (1996). The dynamical evolution of massive black hole binaries I. Hardening in a fixed stellar background. *New Astronomy*, 1, 35–56. [arXiv:astro-ph/9601092](#).
73. Samsing, J., MacLeod, M., & Ramirez-Ruiz, E. (2014). The formation of eccentric compact binary inspirals and the role of gravitational wave emission in binary-single stellar encounters. *Astrophysical Journal*, 784, 71. [arXiv:1308.2964](#).
74. Sesana, A. (2016). The promise of multi-band gravitational wave astronomy. *arXiv e-prints* [arXiv:1602.06951](#).
75. Sesana, A., & Khan, F. M. (2015). Scattering experiments meet N-body - I. A practical recipe for the evolution of massive black hole binaries in stellar environments. *MNRAS*, 454, L66–L70. [arXiv:1505.02062](#).
76. Smith, R. J. E., Mandel, I., & Vechhio, A. (2013). Studies of waveform requirements for intermediate mass-ratio coalescence searches with advanced gravitational-wave detectors. *Physical Review D*, 88(4), 044010. [arXiv:1302.6049](#).
77. Tanay, S., Haney, M., & Gopakumar, A. (2016). Frequency and time-domain inspiral templates for comparable mass compact binaries in eccentric orbits. *Physical Review D*, 93(6), 064031. [arXiv:1602.03081](#).
78. Taniguchi, Y., Shioya, Y., Tsuru, T. G., & Ikeuchi, S. (2000). Formation of intermediate-mass black holes in circumnuclear regions of galaxies. *PASJ*, 52, 533–537. [arXiv:astro-ph/0002389](#).
79. Taracchini, A., Buonanno, A., Pan, Y., Hinderer, T., Boyle, M., Hemberger, D. A., et al. (2014). Effective-one-body model for black-hole binaries with generic mass ratios and spins. *Physical Review D*, 89(6), 061502. [arXiv:1311.2544](#).
80. Tiwari, V., Klimentenko, S., Christensen, N., Huerta, E. A., Mohapatra, S. R. P., Gopakumar, A., Haney, M., Ajith, P., McWilliams, S. T., Vedovato, G., Drago, M., Salemi, F., Prodi, G. A., Lazzaro, C., Tiwari, S., Mitselmakher, G., & Da Silva, F. (2016). Proposed search for the detection of gravitational waves from eccentric binary black holes. *Physical Review D*, 93(4), 043007. [arXiv:1511.09240](#).
81. Trenti, M. (2006). Dynamical evidence for intermediate mass black holes in old globular clusters. *arXiv Astrophysics e-prints* [arXiv:astro-ph/0612040](#).
82. Trenti, M., Ardi, E., Mineshige, S., & Hut, P. (2007a). Star clusters with primordial binaries - III. Dynamical interaction between binaries and an intermediate-mass black hole. *MNRAS*, 374, 857–866. [arXiv:astro-ph/0610342](#).
83. Trenti, M., Heggie, D. C., & Hut, P. (2007b). Star clusters with primordial binaries - II. Dynamical evolution of models in a tidal field. *MNRAS*, 374, 344–356. [arXiv:astro-ph/0602409](#).
84. Umbreit, S., & Rasio, F. A. (2013). Constraining Intermediate-mass black holes in globular clusters. *Astrophysical Journal*, 768, 26. [arXiv:1207.2497](#).
85. Vitale, S. (2016). Multi-band gravitational-wave astronomy: parameter estimation and tests of general relativity with space and ground-based detectors. *arXiv e-prints* [arxiv:1605.01037](#).
86. Wen, L. (2003). On the eccentricity distribution of coalescing black hole binaries driven by the Kozai mechanism in globular clusters. *Astrophysical Journal*, 598, 419–430. [arXiv:astro-ph/0211492](#).

Globular Cluster Binaries and Gravitational Wave
Parameter Estimation

Challenges and Efficient Solutions

Haster, C.-J.

2017, XII, 92 p. 37 illus., 9 illus. in color., Hardcover

ISBN: 978-3-319-63440-1